

Isvector nuclear spin-orbit interaction from chiral pion-nucleon dynamics

N. Kaiser

Physik Department T39, Technische Universität München, D-85747 Garching, Germany

email: nkaiser@physik.tu-muenchen.de

Abstract

Using the two-loop approximation of chiral perturbation theory, we calculate the momentum and density dependent isovector nuclear spin-orbit strength $V_{ls}(p, k_f)$. This quantity is derived from the spin-dependent part of the interaction energy $\Sigma_{spin} = \frac{i}{2} \vec{\sigma} \cdot (\vec{q} \times \vec{p}) [U_{ls}(p, k_f) - V_{ls}(p, k_f) \tau_3 \delta]$ of a nucleon scattering off weakly inhomogeneous isospin-asymmetric nuclear matter. We find that iterated 1π -exchange generates at saturation density, $k_{f0} = 272.7 \text{ MeV}$, an isovector nuclear spin-orbit strength at $p = 0$ of $V_{ls}(0, k_{f0}) \simeq 50 \text{ MeVfm}^2$. This value is about 1.4 times the analogous isoscalar nuclear spin-orbit strength $U_{ls}(0, k_{f0}) \simeq 35 \text{ MeVfm}^2$ generated by the same two-pion exchange diagrams. We also calculate several relativistic $1/M$ -corrections to the isoscalar nuclear spin-orbit strength. In particular, we evaluate the contributions from irreducible two-pion exchange to $U_{ls}(p, k_f)$. The effects of the three-body diagrams constructed from the Weinberg-Tomozawa $\pi\pi NN$ -contact vertex on the isoscalar nuclear spin-orbit strength are computed. We find that such relativistic $1/M$ -corrections are less than 20% of the isoscalar nuclear spin-orbit strength generated by iterated one-pion-exchange, in accordance with the expectation from chiral power counting.

PACS: 12.38.Bx, 21.65.+f, 24.10.Cn

Keywords: Effective field theory at finite density, Isoscalar and isovector nuclear spin-orbit interaction.

1 Introduction

The introduction of the spin-orbit term into the nuclear single-particle Hamiltonian has been most decisive for the success of the nuclear shell model [1]. Only with a very strong and attractive spin-orbit potential one is, for example, able to explain the observed sequence of so-called magic numbers $\{2, 8, 20, 28, 50, 82, 126, \dots\}$. The dynamical origin of the strong nuclear spin-orbit force has not been fully resolved even up to date. The analogy with the spin-orbit interaction in atomic physics gave the hint that it could be a relativistic effect. This idea has led to the construction of the relativistic (scalar-vector) mean-field model [2]. In this model the spin-independent nuclear potential (of approximate depth -50 MeV) results from an almost complete cancelation of a very strong attraction generated by scalar (σ -meson) exchange and a nearly equally strong repulsion generated by vector (ω -meson) exchange. The corresponding spin-orbit term (obtained by a non-relativistic reduction of the nucleon's Dirac-Hamiltonian) comes out proportional to the coherent sum of the very large scalar and vector mean-fields. In this sense, the relativistic mean-field model gives a simple and natural explanation of the basic features of the nuclear shell model potential. Refinements of relativistic mean-field models

which include additional non-linear couplings of the scalar and vector fields or explicitly density-dependent point couplings of nucleons are nowadays widely and successfully used for nuclear structure calculations [3, 4, 5].

The nuclear spin-orbit potential arises generally as a many-body effect from the underlying spin-orbit term in the (free) nucleon-nucleon scattering amplitude. The calculation of the tree level diagrams with one scalar-meson or one vector-meson exchange between nucleons gives indeed a spin-orbit term in the NN T-matrix proportional to $1/M^2$, with M denoting the nucleon mass. The nuclear spin-orbit potential corresponding to scalar and vector meson exchange is therefore obviously a truly relativistic effect. However, the quadratic reciprocal scaling of the spin-orbit NN-amplitude with the nucleon mass M is not universal, and it changes if one considers the exchange of two mesons between nucleons, i.e. loop diagrams. For example, irreducible two-pion exchange gives rise to a spin-orbit term in the NN T-matrix proportional to $1/M$ (see eqs.(22,23) in ref.[6]) and iterated one-pion exchange produces a spin-orbit term in the NN T-matrix which even scales linearly with the nucleon mass M (see eq.(33) in ref.[6]).

In a recent work [7] we have used the systematic framework of chiral perturbation theory to calculate the nuclear spin-orbit interaction generated by one- and two-pion exchange. The momentum and density dependent nuclear spin-orbit strength $U_{ls}(p, k_f)$ is derived from the spin-dependent part of the interaction energy $\Sigma_{spin} = \frac{i}{2} \vec{\sigma} \cdot (\vec{q} \times \vec{p}) U_{ls}(p, k_f)$ of a nucleon scattering off weakly inhomogeneous isospin-symmetric nuclear matter. When working to linear order in small spatial gradients (which corresponds to linear order in the momentum transfer \vec{q}) no detailed knowledge about the density distribution of nuclear matter is required. In fact, after isolating the important proportionality factor \vec{q} from the expressions of self-energy-type diagrams the nuclear spin-orbit strength $U_{ls}(p, k_f)$ can be finally computed in the limit of homogeneous isospin-symmetric nuclear matter (characterized by its Fermi momentum k_f). It was found in ref.[7] that the Hartree and Fock diagrams of iterated one-pion exchange generate a spin-orbit strength at $p = 0$ of $U_{ls}(0, k_{f0}) = 34.7 \text{ MeVfm}^2$ which is in perfect agreement with the empirical value $\tilde{U}_{ls} \simeq 35 \text{ MeVfm}^2$ [9, 10] used in shell-model calculation of nuclei. This novel spin-orbit strength is neither of relativistic nor of short range origin. It is in fact linearly proportional to the nucleon mass M and its inherent range is the pion Compton wavelength $m_\pi^{-1} = 1.46 \text{ fm}$. A strong p -dependence of the nuclear spin-orbit strength $U_{ls}(p, k_{f0})$ arising from iterated 1π -exchange has however been observed in ref.[7]. A further property of the spin-orbit Hamiltonian emerging from that diagrammatic calculation was that it has (in coordinate space) terms proportional to $\vec{\nabla} f(r)$ as well as terms proportional to $f(r) \vec{\nabla} f(r)$ (with $f(r) = \rho(r)/\rho(0)$ the normalized radial density profile) which get weighted differently at the surface of a finite nucleus. All such (unusual) features which go beyond the simple shell model parameterization of the nuclear spin-orbit Hamiltonian leave questions about the ultimate relevance of the spin-orbit interaction generated by 2π -exchange for a finite nucleus. Nuclear structure calculation which use the results of ref.[7] as input are necessary in order to clarify the role of the nuclear spin-orbit interaction generated by 2π -exchange.

The purpose of the present work is to calculate using the same framework as in ref.[7] the isovector spin-orbit strength $V_{ls}(p, k_f)$ generated by iterated 1π -exchange in order to reveal the underlying isospin dependence. Furthermore, we calculate here several relativistic $1/M$ -corrections to the isoscalar nuclear spin-orbit strength $U_{ls}(p, k_f)$. In particular, we evaluate the contributions to $U_{ls}(p, k_f)$ arising from irreducible two-pion exchange. We compute the isoscalar nuclear spin-orbit strength generated by certain three-body diagrams constructed from the leading order isovector chiral $\pi\pi NN$ -contact vertex (so-called Weinberg-Tomozawa vertex). The relativistic $1/M$ -corrections to the dominant Hartree diagrams of iterated 1π -exchange are also calculated. These results shed some light on the convergence of the small momentum expansion underlying the whole approach.

2 General considerations about the nuclear spin-orbit term

Let us begin with recalling the spin-orbit Hamiltonian of the nuclear shell model [9, 10] which is generally written in the form:

$$\mathcal{H}_{ls} = \left(\tilde{U}_{ls} - \tilde{V}_{ls} \tau_3 \delta \right) \frac{\vec{\sigma} \cdot \vec{\ell}}{2r} \frac{df(r)}{dr}. \quad (1)$$

Here, $\vec{\sigma}$ is the conventional Pauli spin-vector and $\vec{\ell} = \vec{r} \times \vec{p}$ is the orbital angular momentum of a nucleon. $f(r)$ denotes the normalized radial density distribution of a nucleus, typically parameterized by a Saxon-Woods function. $\delta = (N - Z)/(N + Z)$ is the isospin asymmetry parameter and $\tau_3 \rightarrow \pm 1$ for a proton or a neutron. The empirical value of the isoscalar nuclear spin-orbit strength is $\tilde{U}_{ls} \simeq 35 \text{ MeVfm}^2$ [9, 10]. The ratio of the isovector and isoscalar nuclear spin-orbit strengths $\tilde{V}_{ls}/\tilde{U}_{ls} \simeq -0.6$ is commonly assumed to be equal to the ratio of the spin-independent isovector and isoscalar average nuclear potentials [9, 10].

We wish to calculate the nuclear spin-orbit strengths \tilde{U}_{ls} and \tilde{V}_{ls} (or appropriate generalization of them) in the systematic framework of in-medium chiral perturbation theory [8]. The first observation one makes is that the spin-orbit interaction vanishes identically in infinite homogeneous nuclear matter since there is no preferred center in this system in order to define an orbital angular momentum. Therefore one has to generalize the calculation of the single-particle potential in ref.[8] to (at least) weakly inhomogeneous nuclear matter. The relevant quantity in order to extract the isoscalar and isovector nuclear spin-orbit strengths is the spin-dependent part of the interaction energy of a nucleon scattering off weakly inhomogeneous isospin-asymmetric nuclear matter from initial momentum $\vec{p} - \vec{q}/2$ to final momentum $\vec{p} + \vec{q}/2$, which reads:

$$\Sigma_{spin} = \frac{i}{2} \vec{\sigma} \cdot (\vec{q} \times \vec{p}) \left\{ U_{ls}(p, k_f) - V_{ls}(p, k_f) \tau_3 \delta + \mathcal{O}(\delta^2) \right\}. \quad (2)$$

The (small) momentum transfer \vec{q} is provided by the Fourier-components of the inhomogeneous nuclear matter distribution. The density form factor $\Phi(\vec{q}) = \int d^3r e^{-i\vec{q}\cdot\vec{r}} f(r)$ plays the role of a probability distribution of these Fourier-components. With the help of this relationship the spin-orbit Hamiltonian \mathcal{H}_{ls} in eq.(1) becomes equal to the Fourier-transform of the product of the density form factor $\Phi(\vec{q})$ and the spin-dependent interaction energy Σ_{spin} : $\mathcal{H}_{ls} = (2\pi)^{-3} \int d^3q e^{i\vec{q}\cdot\vec{r}} \Phi(\vec{q}) \Sigma_{spin}$.



Fig.1: The double line symbolizes the medium insertion for a weakly inhomogeneous many-nucleon system $\Gamma(\vec{p}_j, \vec{q}_j)$ defined by eqs.(3,4). Right: The 1π -exchange Fock graph.

Consistent with the assumption of a weakly inhomogeneous nuclear matter distribution we keep in Σ_{spin} only linear terms in \vec{q} corresponding to small spatial gradients of the density profile $f(r)$. Practically, this means that after isolating the proportionality factor \vec{q} in an explicit calculation one can take the limit of homogeneous isospin-asymmetric nuclear matter characterized by its proton and neutron Fermi momenta $k_{p,n} = k_f(1 \mp \delta)^{1/3}$. The expansion up to linear order in the isospin asymmetry parameter δ gives then the momentum and density dependent isoscalar and isovector nuclear spin-orbit strengths $U_{ls}(p, k_f)$ and $V_{ls}(p, k_f)$. Possible higher powers in \vec{q} contributing to Σ_{spin} have no direct correspondence to the (standard) spin-orbit Hamiltonian \mathcal{H}_{ls} in eq.(1).

In ref.[8] the calculation of the spin-independent single-particle potential in homogeneous isospin-symmetric nuclear matter has been organized in the number of so-called medium insertions. The medium insertion for a (non-relativistic) many-fermion system is generally constructed from the sum over the occupied energy eigenstates as [11, 12]:

$$\Gamma(\vec{p}_j, \vec{q}_j) = \int d^3r_1 \int d^3r_2 \sum_{E \in occ} \psi_E(\vec{r}_2) \psi_E^*(\vec{r}_1) e^{i\vec{p}_j \cdot (\vec{r}_1 - \vec{r}_2)} e^{-\frac{i}{2}\vec{q}_j \cdot (\vec{r}_1 + \vec{r}_2)}. \quad (3)$$

The double line in the left picture of Fig. 1 symbolized this medium insertion together with the assignment of the out- and in-going nucleon momenta $\vec{p}_j \pm \vec{q}_j/2$. The momentum transfer \vec{q}_j is provided by the Fourier-components of the inhomogeneous matter distribution. Semi-classical expansions [11, 12] give for a weakly inhomogeneous and spin-saturated many-nucleon system:

$$\Gamma(\vec{p}_j, \vec{q}_j) = \left[\frac{1 + \tau_3}{2} \theta(k_p - |\vec{p}_j|) + \frac{1 - \tau_3}{2} \theta(k_n - |\vec{p}_j|) \right] \Phi(\vec{q}_j) \{1 + \mathcal{O}(\vec{q}_j)\}, \quad (4)$$

with $\Phi(\vec{q}_j)$ the density form factor introduced after eq.(2). The subleading $\mathcal{O}(\vec{q}_j)$ term in eq.(4) will never come into play in the calculation of the spin-dependent interaction energy Σ_{spin} to linear order in \vec{q} .

3 Diagrammatic calculation of the isovector nuclear spin-orbit strength

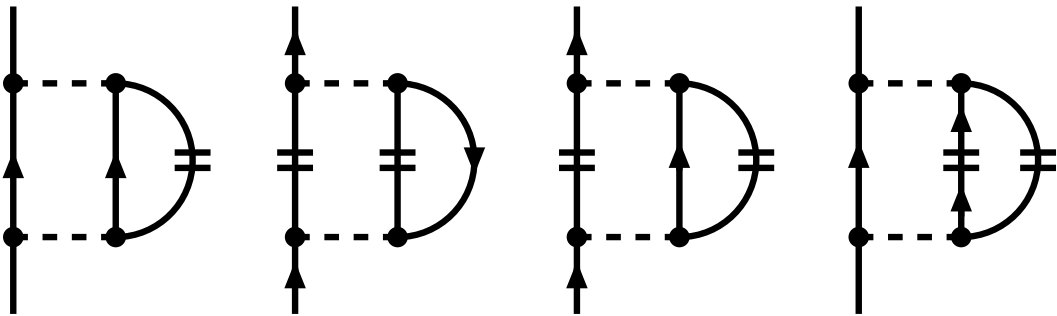


Fig.2: The iterated 1π -exchange Hartree graphs. These diagrams are labeled (a), (b), (c), (d) from left to right.

In this section we present analytical results for the isovector nuclear spin-orbit strength $V_{ls}(p, k_f)$ as given by chiral one- and two-pion exchange. We start with the 1π -exchange Fock¹

¹Our nomenclature of "Hartree" and "Fock" diagrams is taken over from ref.[8]. There closed 1π - and 2π -exchange vacuum diagrams with two (resp. one) closed nucleon line have been called Hartree (resp. Fock) diagrams. The one-particle property Σ_{spin} is obtained by opening one nucleon line of such diagrams. Consequently, we call here diagrams with one open and one closed nucleon line "Hartree" diagrams and diagrams with only one open nucleon line "Fock" diagrams.

graph (right diagram in Fig. 1). In the static approximation the product of πN -interaction vertices $\vec{\sigma} \cdot (\vec{p} - \vec{p}_1) \vec{\sigma} \cdot (\vec{p} - \vec{p}_1) = (\vec{p} - \vec{p}_1)^2$ is spin-independent. A non-vanishing nuclear spin-orbit strength comes therefore only as a relativistic $1/M^2$ -correction. Isolating the $i \vec{\sigma} \times \vec{q}$ factor from the product of fully relativistic pseudo-vector πN -interaction vertices, performing the $1/M$ -expansion, integrating over Fermi-spheres of radii $k_{p,n} = k_f(1 \mp \delta)^{1/3}$ and expanding to linear order in the asymmetry parameter δ , we get from the 1π -exchange Fock diagram:

$$V_{ls}^{(1\pi)}(p, k_f) = \frac{2g_A^2 m_\pi^3 u^2 (u^2 - x^2)}{3(8\pi f_\pi M x)^2} \left\{ (1 + u^2 - x^2)L(x, u) - u \right\}. \quad (5)$$

Here, we have introduced the dimensionless variables $x = p/m_\pi$ and $u = k_f/m_\pi$ and the auxiliary function

$$L(x, u) = \frac{1}{4x} \ln \frac{1 + (u + x)^2}{1 + (u - x)^2}. \quad (6)$$

Next, we come to the evaluation of the four Hartree diagrams of iterated one-pion exchange shown in Fig. 2. We start with the left graph with one medium insertion, labeled (a). The relevant $i \vec{\sigma} \times \vec{q}$ prefactor can be isolated already in the first step of the calculation from the product of πN -interaction vertices $\vec{\sigma} \cdot (\vec{l} - \vec{q}/2) \vec{\sigma} \cdot (\vec{l} + \vec{q}/2)$ at the open nucleon line. For all remaining parts of that diagram one can then take the limit of homogeneous isospin-asymmetric nuclear matter (i.e. $\vec{q} = 0$). After solving the inner d^3l -loop integral [6] and expanding the integrals over Fermi spheres of radii $k_{p,n} = k_f(1 \mp \delta)^{1/3}$ to linear order in δ , we find the following closed form expression for the isovector nuclear spin-orbit strength generated by the Hartree diagram (a):

$$V_{ls}^{(a)}(p, k_f) = \frac{g_A^4 M m_\pi^2 u^2}{(4\pi x)^3 f_\pi^4} \left\{ \frac{8u}{3} \left[\arctan(u-x) - \arctan(u+x) \right] + 2x \left(\frac{5}{3} - u^2 + x^2 \right) L(x, u) + 2ux \right\}. \quad (7)$$

We continue with the calculation of the Hartree diagrams with two medium insertions, labeled (b), (c) and (d) in Fig. 2. In these diagrams, a (small) momentum transfer $\vec{q}_{1,2}$ with $\vec{q} = \vec{q}_1 + \vec{q}_2$ occurs at each medium insertion. The important prefactors $i \vec{\sigma} \times \vec{q}_j$ can again be isolated in the first step of the calculation from the product of πN -interaction vertices at the open nucleon line. After that the vectors \vec{q}_j can be set to zero in all remaining components of these diagrams. When Fourier-transformed with density form factors to coordinate space each such momentum transfer \vec{q}_j , ($j = 1, 2$) leads to the expression: $(2\pi)^{-6} \int d^3q \int d^3q_j e^{i\vec{q}\cdot\vec{r}} i\vec{q}_j \Phi(\vec{q}_j) \Phi(\vec{q} - \vec{q}_j) = f(r) \vec{\nabla} f(r)$, with $f(r)$ the density profile of weakly inhomogeneous nuclear matter. Consistent with the assumption of a weakly inhomogeneous nuclear matter (i.e. keeping only linear terms in small spatial gradients) we can make the replacement: $f(r) \vec{\nabla} f(r) \rightarrow \vec{\nabla} f(r)$. The essential conclusion from this consideration is that for the calculation of Σ_{spin} in weakly inhomogeneous nuclear matter each momentum transfer \vec{q}_j can be identified with \vec{q} . With the help of this rule and certain techniques to reduce six-dimensional principal value integrals over the product of two Fermi-spheres, we end up after expanding to linear order in δ with the following result for the Hartree diagram (b):

$$V_{ls}^{(b)}(p, k_f) = \frac{g_A^4 M m_\pi^2}{(4\pi f_\pi)^4} \int_{-1}^1 dy \frac{4y}{3x} \left\{ 2u^2 \left[\frac{3s + 2s^3}{1 + s^2} - 3 \arctan s \right] \ln \frac{u + xy}{u - xy} - \frac{s'^4}{(1 + s^2)^2} \left[2uxy + (u^2 - x^2 y^2) \ln \frac{u + xy}{u - xy} \right] \right\} \quad (8)$$

with the auxiliary functions $s = xy + \sqrt{u^2 - x^2 + x^2 y^2}$ and $s' = u \partial s / \partial u$. Throughout this work the momentum p is restricted to the interval $0 \leq p \leq k_f$. Similarly, we find for the Hartree

diagram (c):

$$V_{ls}^{(c)}(p, k_f) = \frac{g_A^4 M m_\pi^2}{(4\pi f_\pi)^4} \int_{-1}^1 dy \int_{-xy}^{s-xy} d\xi \frac{4y(xy + \xi)^4}{3sx[1 + (xy + \xi)^2]^2} \left\{ s'(3\xi + 2xy) \left[\xi \ln \frac{u + \xi}{u - \xi} - 2u \right] \right. \\ \left. - \frac{4s'}{1 + (xy + \xi)^2} \left[2u\xi + (u^2 - \xi^2) \ln \frac{u + \xi}{u - \xi} \right] - (4s + s')u^2 \ln \frac{u + \xi}{u - \xi} \right\}, \quad (9)$$

and for the Hartree diagram (d):

$$V_{ls}^{(d)}(p, k_f) = \frac{g_A^4 M m_\pi^2}{(2\pi f_\pi)^4} \int_0^u d\xi \frac{2\xi^2}{3x^3} \int_{-1}^1 dy \left\{ \frac{x^3}{x^2 - \xi^2 y^2} \left[\frac{3\sigma + 2\sigma^3}{1 + \sigma^2} - 3 \arctan \sigma \right] \right. \\ \left. + \left[\xi y \ln \frac{|x + \xi y|}{|x - \xi y|} - 2x \right] \left[\frac{\sigma(1 - 2\sigma^3 \sigma')}{(1 + \sigma^2)^2} + 5\sigma - 6 \arctan \sigma \right] \right\}, \quad (10)$$

with the auxiliary functions $\sigma = \xi y + \sqrt{u^2 - \xi^2 + \xi^2 y^2}$ and $\sigma' = u \partial \sigma / \partial u$. The symbol $\int_{-1}^1 dy$ in eq.(10) stands for a principal value integral. Note the similarity of the expressions eqs.(8,9,10) with the three-body isovector single-particle potentials written in eqs.(30,31,32) of ref.[7].

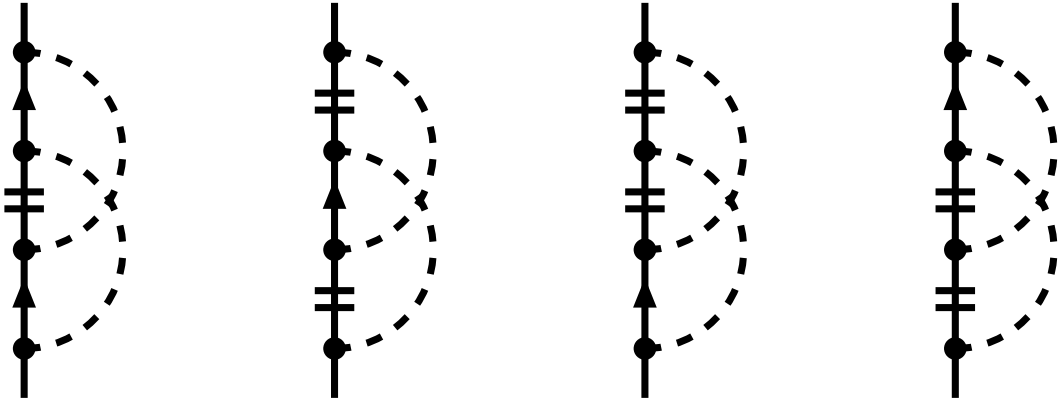


Fig.3: The iterated 1π -exchange Fock graphs. These diagrams are labeled (e), (f), (g), (g) from left to right.

Next, we come to the evaluation of the four iterated 1π -exchange Fock diagrams shown in Fig.3. We start with diagram (e) with one medium insertion. The method to isolate the important proportionality factor \vec{q} has been explained in section 3 of ref.[7]. Considering the isospin factor of diagram (e) and expanding the integrals over Fermi spheres of radii $k_{p,n} = k_f(1 \mp \delta)^{1/3}$ to linear order in the asymmetry parameter δ , we end up with the following contribution to the isovector nuclear spin-orbit strength:

$$V_{ls}^{(e)}(p, k_f) = \frac{5g_A^4 M m_\pi^2 u^2}{3(8\pi x)^3 f_\pi^4} \left\{ 2(u^2 - x^2) \ln \frac{u + x}{u - x} - 4ux + \int_{(u-x)/2}^{(u+x)/2} d\xi \frac{4\xi^2 + x^2 - u^2}{\xi^2(1 + 2\xi^2)} \right. \\ \left. \times \left[(1 + 4\xi^2) \arctan 2\xi - 4\xi^2(1 + \xi^2) \arctan \xi \right] \right\}. \quad (11)$$

We continue with the computation of the Fock diagram (f) with a symmetrical arrangement of the two medium insertions. It leads to the following contribution to the isovector nuclear spin-orbit strength:

$$V_{ls}^{(f)}(p, k_f) = \frac{g_A^4 M m_\pi^2}{(4\pi f_\pi)^4} \left\{ \frac{u^2}{3x^4} G(x, u) \left[(u^2 + 1 - 2x^2) L(x, u) - u \right] \right.$$

$$\begin{aligned}
& + \frac{u}{12x^4} \frac{\partial G(x, u)}{\partial u} \left[2x^2 \left(\arctan(u+x) + \arctan(u-x) \right) \right. \\
& \left. - u(1+u^2+3x^2) + \left((1+u^2)^2 + x^2(3x^2-4u^2) \right) L(x, u) \right] \\
& + \int_{-1}^1 dy \int_{-1}^1 dz \frac{yz \theta(y^2+z^2-1)}{3x|yz|\sqrt{y^2+z^2-1}} \frac{s^2 s'}{1+s^2} \\
& \times \left[2sz(t - \arctan t) + y(t^2 - \ln(1+t^2)) \right] \Big\}, \tag{12}
\end{aligned}$$

with the auxiliary functions $G(x, u) = u(1+u^2+x^2) - [1+(u+x)^2][1+(u-x)^2]L(x, u)$ and $t = xz + \sqrt{u^2 - x^2 + x^2 z^2}$. Finally, we have to evaluate the last two topologically distinct Fock diagrams in Fig. 3. Since they contribute equally to the spin-dependent interaction energy Σ_{spin} we have given both diagrams the same label (g). We find the following representation for their contribution to the isovector nuclear spin-orbit strength:

$$V_{ls}^{(g)}(p, k_f) = -\frac{g_A^4 M m_\pi^2 u}{6x^3 (4\pi f_\pi)^4} \left[H(x, u, u) + 5 \int_0^u d\xi \frac{\partial H(x, u, \xi)}{\partial u} \right]. \tag{13}$$

Here, we have introduced the abbreviation:

$$\begin{aligned}
H(x, u, \xi) = & 3ux\xi^{-2}(1+u^2)(1+\xi^2) - ux(12\xi^2+1+x^2) \\
& + 8\xi^2 \left[\arctan(u+\xi) + \arctan(u-\xi) \right] \left[x + (x^2-1-\xi^2)L(\xi, x) \right] \\
& + \left[3\xi^4(4u^2+5x^2-3) + \xi^2(5+10u^2-4x^2-14u^2x^2-x^4) - 12\xi^6 - 2u^2x^4 \right. \\
& \left. + 5 + 3u^4 + 3x^2 - u^4x^2 + 4u^2 + 2x^4 - 6u^2x^2 + 3\xi^{-2}(1+u^2)^2(1+x^2)^2 \right] \\
& \times L(\xi, x)L(\xi, u) + \left[12\xi^4 + \xi^2(x^2-12u^2-3) + 2(1+x^2)(u^2-1) \right. \\
& \left. - 3\xi^{-2}(1+x^2)(1+u^2)^2 \right] xL(\xi, u) + \left[12\xi^4 + \xi^2(13-15x^2) \right. \\
& \left. + x^4 + u^2x^2 + 3x^2 - 3u^2 - 2 - 3\xi^{-2}(1+x^2)^2(1+u^2) \right] uL(\xi, x) \\
& + \xi^2 \int_{-1}^1 dy \left\{ 16(\sigma - \arctan \sigma)[x - L(\xi, x)] \right. \\
& + \left[\ln(1+\sigma^2) + 8\xi y \arctan \sigma + 4u^2 - 4\xi^2 - 5\sigma^2 \right] \ln \frac{|x+\xi y|}{|x-\xi y|} \\
& + \left[8\xi y \arctan \sigma + (1+\xi^2-x^2)\ln(1+\sigma^2) + 4u^2 - 4\xi^2 \right. \\
& \left. + \sigma^2(x^2-5-\xi^2) \right] \frac{1}{R} \ln \frac{|xR+(x^2-1-\xi^2)\xi y|}{|xR+(1+\xi^2-x^2)\xi y|} \Big\}, \tag{14}
\end{aligned}$$

for the combined integrand of eqs.(21,23) in ref.[7] as well as the auxiliary function $R = \sqrt{(1+x^2-\xi^2)^2 + 4\xi^2(1-y^2)}$. This completes the presentation of analytical results for the isovector nuclear spin-orbit strength $V_{ls}(p, k_f)$ generated by 1π -exchange and iterated 1π -exchange.

3.1 Results

For the numerical evaluation of the isovector nuclear spin-orbit strength $V_{ls}(p, k_f)$ we use consistently the same parameters as in our previous works [7, 8]. We choose the value $g_A = 1.3$ for the nucleon axial vector coupling constant. The weak pion decay constant has the value $f_\pi = 92.4$ MeV and $M = 939$ MeV and $m_\pi = 135$ MeV are the masses of the nucleon and the (neutral) pion, respectively.

Diagram	1 π -Fock	(a)	(b)	(c)	(d)	(e)	(f)	(g)
$V_{ls}(0, k_{f0})$	-0.14	24.72	-1.49	-18.94	51.40	-42.35	-4.55	41.94
$V_{ls}(k_{f0}, k_{f0})$	0.00	22.03	10.60	-10.64	25.83	-38.40	-2.68	27.04

Table 1: Contributions of individual diagrams to the isovector nuclear spin-orbit strength $V_{ls}(p, k_{f0})$ at $p = 0$ and at $p = k_{f0} = 272.7$ MeV. The units are MeVfm².

In the second row of Table 1, we present numerical values for the contributions of individual diagrams to the isovector nuclear spin-orbit strength $V_{ls}(0, k_{f0})$ at the nuclear matter saturation density $k_{f0} = 272.7$ MeV (as predicted by our calculation [8]). As expected the relativistic $1/M^2$ -correction from the 1π -exchange Fock graph is a very small effect. The contributions of individual iterated 1π -exchange diagrams are large and comparable in magnitude to the respective contributions to the isoscalar nuclear spin-orbit strength $U_{ls}(0, k_{f0})$ (see Table 1 in ref.[7]). The basic reason for these large values is the large scale enhancement factor M (the nucleon mass) entering the iterated 1π -exchange. It stems from the energy denominator of such second-order diagrams which is a difference of small nucleon kinetic energies. Adding up the entries in the second row of Table 1 one gets $V_{ls}(0, k_{f0}) = 50.6$ MeVfm², which is about 1.4 times the isoscalar nuclear spin-orbit strength $U(0, k_{k0}) = 35.1$ MeVfm² [7] generated by the same 2π -exchange diagrams. The predicted total sum is dominated by the contribution $V_{ls}^{(H)}(0, k_{f0}) = 55.7$ MeVfm² of the four Hartree diagrams (a), (b), (c) and (d) (see Fig. 2). The same feature, namely the numerical suppression of the iterated 1π -exchange Fock diagrams against the Hartree diagrams, holds also for the isoscalar spin-orbit strength $U_{ls}(0, k_{f0})$ [7] as well as for the (spin-independent) nuclear mean-field studied in ref.[8]. The numerical entries (a)-(g) in Table 1 are all of the same order in the small momentum expansion. Individual cancelations give therefore no hint on the "convergence" of the chiral expansion of $V_{ls}(p, k_f)$. Note that the isovector nuclear spin-orbit strength $V_{ls}(0, k_{f0})$ generated (almost completely) by iterated 1π -exchange is neither of relativistic nor of short range origin. It is in fact linearly proportional to the nucleon mass M and its inherent range is the pion Compton wavelength $m_\pi^{-1} = 1.46$ fm. The full pion Compton wavelength m_π^{-1} and not half of it is suggested by comparing the expression $V_{ls}^{(a)}(p, k_f)$ in eq.(7) with the 1π -exchange single-particle potential $U_2(p, k_f)$ in eq.(8) of ref.[8]. As a matter of fact the same non-polynomial functions $L(x, u)$ and $\arctan(u \pm x)$ occur in both cases.

In Fig. 4, we show by the full line the dependence of the calculated isovector nuclear spin-orbit strength $V_{ls}(0, k_f)$ on the nucleon density $\rho = 2k_f^3/3\pi^2$. One observes in the region $\rho \leq 0.4$ fm⁻³ an approximate linear growth of $V_{ls}(0, k_f)$ with the density ρ as it is typical for relativistic mean-field models. In a finite nucleus the spin-orbit force acts mainly on the surface where the density gradients are largest and the density has dropped to about half of the central density. The replacement $f(r) \vec{\nabla} f(r) \rightarrow \frac{1}{2} \vec{\nabla} f(r)$ (instead of $f(r) \vec{\nabla} f(r) \rightarrow \vec{\nabla} f(r)$ valid for weakly inhomogeneous nuclear matter) describes then more realistically the situation for a finite nucleus. The dashed line in Fig. 4 shows the isovector nuclear spin-orbit strength which results if the contributions from the diagrams with two medium insertion (b), (c), (d), (f) and (g) are weighted with a factor 1/2. This different weighting reduces of the total isovector spin-orbit strength by about a factor 3.

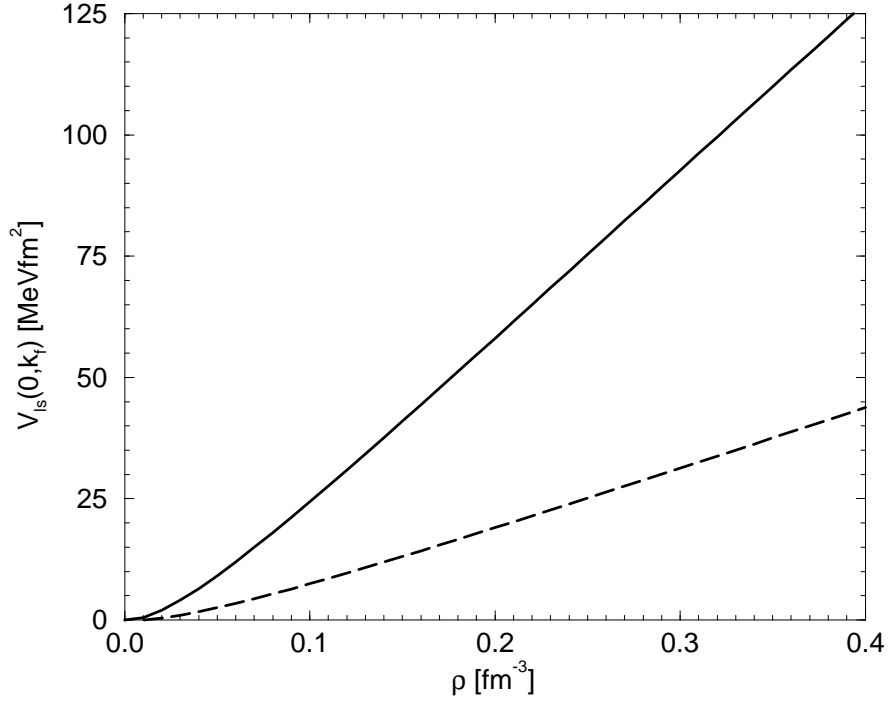


Fig. 4: The full line shows the isovector nuclear spin-orbit strength $V_{ls}(0, k_f)$ at zero nucleon momentum ($p = 0$) versus the nucleon density $\rho = 2k_f^3/3\pi^2$. If the diagrams with two medium insertions are weighted with a factor $1/2$ the dashed line results.

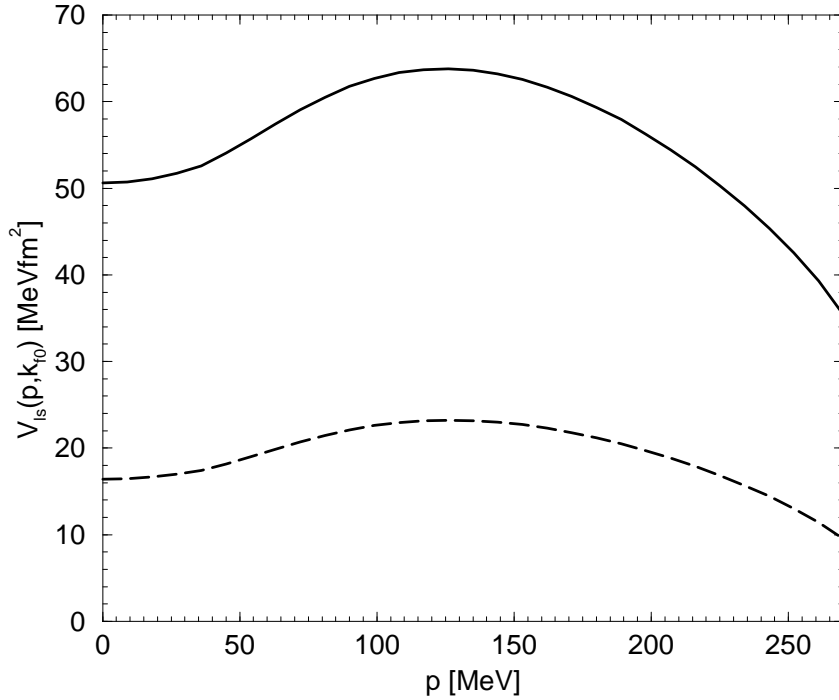


Fig. 5: The momentum dependence of the isovector nuclear spin-orbit strength $V_{ls}(p, k_{f0})$ at saturation density $k_{f0} = 272.7$ MeV. The full (dashed) line corresponds to a weighting of the diagrams with two medium insertions with a factor 1 ($1/2$).

In Fig. 5, we show by the full line the dependence of the calculated isovector nuclear spin-orbit strength $V_{ls}(p, k_{f0})$ at saturation density $k_{f0} = 272.7$ MeV on the nucleon momentum p for $0 \leq p \leq k_{f0}$. One observes a moderate p -dependence. In contrast to the isoscalar nuclear spin-orbit strength $U_{ls}(p, k_{f0})$ shown in Fig. 7 of ref.[7] there is no sign change in the present case.

The dashed line in Fig. 5 corresponds to the weighting of diagrams with two medium insertions with a factor $1/2$. It shows the same qualitative p -dependence as the full line in Fig. 7. The entries in the third row of Table 1 indicate how the contributions from individual diagrams vary with the nucleon momentum from $p = 0$ to $p = k_{f0}$.

The terms from iterated 1π -exchange written down in eqs.(7–14) are the unique leading order contributions in the small momentum expansion. They are of second order in small momenta as signaled by the common prefactor $g_A^4 M m_\pi^2 / (2\pi f_\pi)^4$. Nuclear structure calculations which use the here calculated isovector nuclear spin-orbit strength $V_{ls}(p, k_f)$ as input would be most useful in order to clarify the role of the spin-orbit interaction generated by 2π -exchange in a finite nucleus.

4 Relativistic corrections to the isoscalar nuclear spin-orbit strength

In this section we calculate several higher order corrections to the isoscalar nuclear spin-orbit strength $U_{ls}(p, k_f)$ generated by 2π -exchange in order to learn about the convergence of the underlying small momentum expansion. All these contributions scale like $1/M$ with nucleon mass M and can therefore be regarded as truly relativistic spin-orbit effects. Since our calculation is a strictly perturbative one πN -interaction vertices in-medium are the same as in vacuum. The relativistic spin-orbit effects depend therefore reciprocally on the free nucleon mass M and not on a self-consistently determined effective nucleon mass M^* as it is the case in relativistic mean-field models [2].

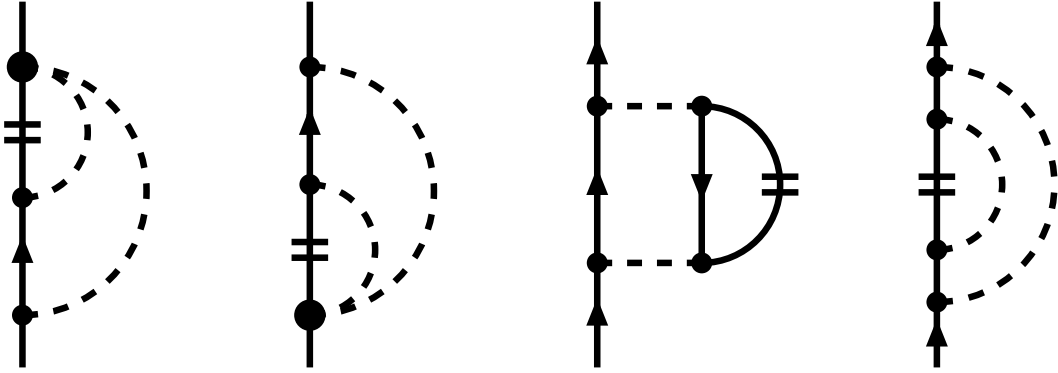


Fig. 6: Some diagrams representing the isoscalar nuclear spin-orbit interaction arising from irreducible two-pion exchange. The first two (last two) diagrams are constructed from the 2π -exchange triangle (crossed box) graph of elastic NN-scattering.

In Fig. 6 we show some diagrams which generate the isoscalar nuclear spin-orbit strength related to irreducible two-pion exchange. By opening them at the medium insertion (symbolized by the double line) ones see that the first two Fock diagrams stem from the 2π -exchange triangle graph of elastic NN-scattering, whereas the last two Hartree and Fock diagrams are constructed from the 2π -exchange crossed box graph of elastic NN-scattering. We have explicitly calculated the isoscalar nuclear spin-orbit strength $U_{ls}(p, k_f)$ generated by these diagrams using the techniques outlined in section 2. In an intermediate step the resulting isoscalar nuclear spin-orbit strength $U_{ls}(p, k_f)$ can be written as an integral of the spin-orbit NN-amplitudes of the triangle and crossed box graph [6] over a Fermi sphere of radius k_f . This expression can be further reduced to a one-dimensional integral of the form:

$$U_{ls}^{(2\pi)}(p, k_f) = \frac{1}{16\pi^2 p^3} \int_{k_f-p}^{k_f+p} dq q [k_f^2 - (p+q)^2][k_f^2 - (p-q)^2] \{V_{SO}(q) + 3W_{SO}(q) + 2V_{SO}(0)\}, \quad (15)$$

with $V_{SO}(q)$ and $W_{SO}(q)$ the isoscalar and isovector spin-orbit NN-amplitudes. The term $2V_{SO}(0)$ in eq.(15) belongs to Hartree type diagrams (with one closed and one open nucleon line) while the term $V_{SO}(q) + 3W_{SO}(q)$ summarizes the contributions from Fock type diagram (having just one open nucleon line). The spin-orbit NN-amplitudes related to irreducible 2π -exchange have been calculated in section 4.2 of ref.[6] using dimensional regularization. If we use instead cut-off regularization the linear divergences of the irreducible 2π -exchange diagrams become visible. We find:

$$V_{SO}(q) = \frac{3g_A^4}{64\pi M f_\pi^4} \left\{ -\frac{11\Lambda}{6\pi} + m_\pi + \frac{2m_\pi^2 + q^2}{2q} \arctan \frac{q}{2m_\pi} \right\}, \quad (16)$$

$$W_{SO}(q) = \frac{g_A^2}{64\pi M f_\pi^4} \left\{ \frac{(7g_A^2 - 8)\Lambda}{3\pi} + (1 - g_A^2) \left[m_\pi + \frac{4m_\pi^2 + q^2}{2q} \arctan \frac{q}{2m_\pi} \right] \right\}, \quad (17)$$

which agrees up to the additive constants linear in the momentum cut-off Λ with the expressions in eqs.(22,23) of ref.[6]. Note that eqs.(16,17) include also the irreducible contributions of the 2π -exchange planar box graph (not shown in Fig.6). Inserting eqs.(16,17) into the "master formula" eq.(15) one gets for isoscalar nuclear spin-orbit strength arising from irreducible two-pion exchange:

$$\begin{aligned} U_{ls}^{(2\pi)}(p, k_f) &= \frac{g_A^2 \Lambda k_f^3}{3M(2\pi f_\pi)^4} \left(2 + \frac{19g_A^2}{8} \right) + \frac{g_A^2 m_\pi^4}{35M(8\pi x)^3 f_\pi^4} \left\{ \left[24(7g_A^2 - 4) \right. \right. \\ &+ 28(5g_A^2 - 4)(u^2 + x^2) + 35 \left(\frac{3g_A^2}{2} - 2 \right) (u^2 - x^2)^2 \left. \right] \ln \frac{4 + (u + x)^2}{4 + (u - x)^2} \\ &+ 2(u + x)^3 \left[(u^2 - 3ux + x^2)(28 - 14g_A^2 + u^2 + x^2) - 10u^2 x^2 \right] \arctan \frac{u + x}{2} \\ &+ 2(x - u)^3 \left[(u^2 + 3ux + x^2)(28 - 14g_A^2 + u^2 + x^2) - 10u^2 x^2 \right] \arctan \frac{u - x}{2} \\ &+ 2ux \left[12(4 - 7g_A^2) + (44 - 49g_A^2)(u^2 + x^2) \right. \\ &\left. \left. - 4(u^4 + x^4 + (22 + 105g_A^2)u^2 x^2) \right] \right\}. \quad (18) \end{aligned}$$

At zero nucleon momentum ($p = 0$) this simplifies to:

$$\begin{aligned} U_{ls}^{(2\pi)}(0, k_f) &= \frac{g_A^2 \Lambda k_f^3}{3M(2\pi f_\pi)^4} \left(2 + \frac{19g_A^2}{8} \right) \\ &+ \frac{g_A^2 k_f^2}{(4\pi)^3 M f_\pi^4} \left\{ - (3g_A^2 + 1)m_\pi k_f + \left[(g_A^2 - 2)m_\pi^2 - \frac{k_f^2}{2} \right] \arctan \frac{k_f}{2m_\pi} \right\}. \quad (19) \end{aligned}$$

Note the reciprocal dependence on the nucleon mass M which indicates that this nuclear spin-orbit strength is a relativistic effect.

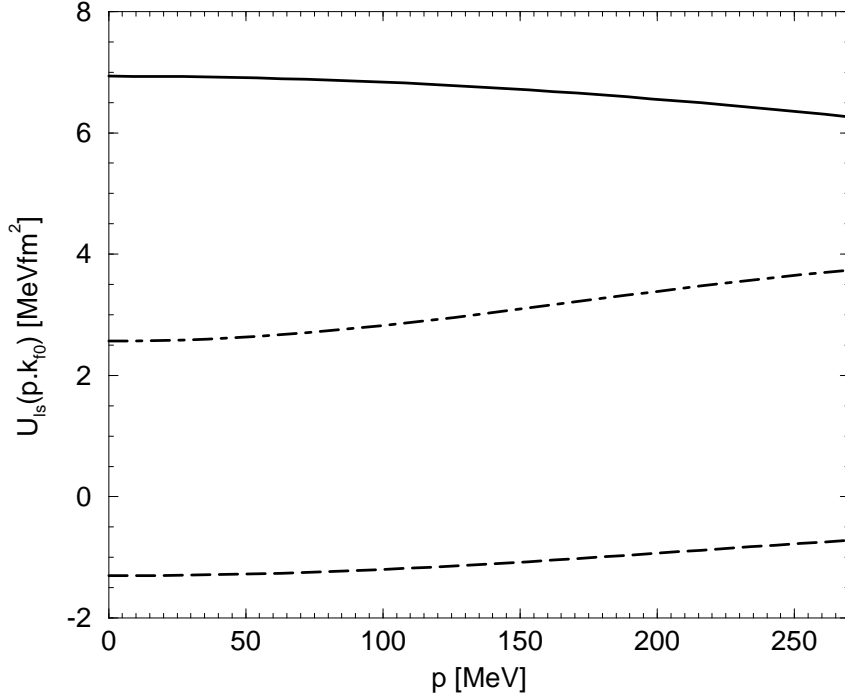


Fig. 7: The full line shows the isoscalar nuclear spin-orbit strength $U_{ls}^{(2\pi)}(p, k_{f0})$ related to irreducible 2π -exchange versus the nucleon momentum p . The dashed line gives the combined result of the three-body diagrams in Fig. 8 and the dashed-dotted line corresponds to the relativistic $1/M$ -correction to the iterated 1π -exchange Hartree diagram (a) in Fig. 2.

As in our previous work [8] we choose the value $\Lambda \simeq 0.65$ GeV for the momentum cutoff Λ . This gives at saturation density $k_{f0} = 272.7$ MeV an isoscalar nuclear spin-orbit strength due to irreducible 2π -exchange of $U_{ls}^{(2\pi)}(0, k_{f0}) = (16.20 - 9.27) \text{ MeVfm}^2 = 6.93 \text{ MeVfm}^2$. This combination of Λ -dependent and finite terms is less than 20% of the total isoscalar spin-orbit strength coming from iterated 1π -exchange. Such a reduction factor is in accordance with the expectations from chiral power counting since the first/second term of $U_{ls}^{(2\pi)}(0, k_f)$ in eq.(19) is suppressed by one/two powers of small momenta in comparison to the results from iterated 1π -exchange. The full line in Fig. 7 shows the momentum dependence of the isoscalar nuclear spin-orbit strength $U_{ls}^{(2\pi)}(p, k_{f0})$. One observes a very weak fall-off with momentum from $p = 0$ to $p = k_{f0} = 272.7$ MeV.

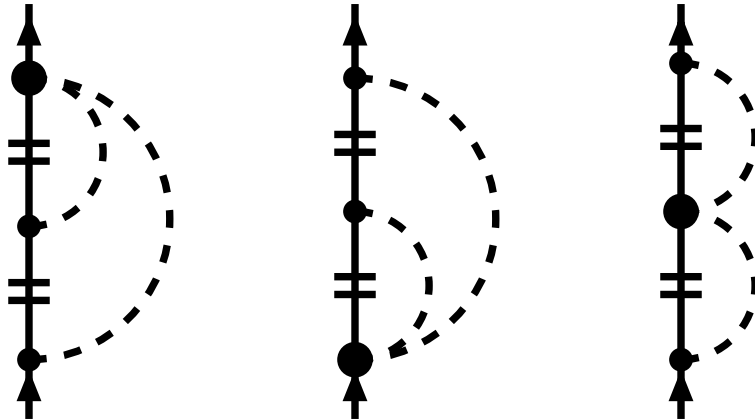


Fig. 8: Three-body force Fock diagrams constructed from the (isovector) Weinberg-Tomozawa $\pi\pi NN$ -contact vertex. Analogous Hartree diagrams which have an isospin factor zero in isospin-symmetric nuclear matter are not shown.

By putting a second medium insertion to the intermediate nucleon propagator in the first two diagrams in Fig.6 the first two graphs shown in Fig.8 result. By opening them at the two medium insertions one sees that these graphs can be classified as three-body diagrams. With employment of one (isovector) Weinberg-Tomozawa $\pi\pi NN$ -contact vertex one can construct a tree-level 2π -exchange three-body diagram (NNN \rightarrow NNN). The three Fock diagrams in Fig.8 result then from this three-body diagram by closing two nucleon lines in all possible ways.² Let us begin with the computation of the right Fock diagram in Fig.8 having a symmetrical arrangement of the two medium insertions. The $\pi\pi NN$ -contact vertex (symbolized by the heavy dot) contributes for the relevant kinematics first in form of a relativistic $1/M$ -correction. After isolating the proportionality factor $i\vec{\sigma} \times \vec{q}$ from all spin-dependent terms one is left with an integral over the product of two Fermi spheres of radius k_f . The latter can be solved in closed form and one gets the following contribution from the third diagram in Fig.8 to the isoscalar nuclear spin-orbit strength:

$$\begin{aligned}
U_{ls}^{(3)}(p, k_f) = & \frac{g_A^2 m_\pi^4 G(x, u)}{24M(4\pi f_\pi x)^4} \left\{ u \left[x^2(24 + 3x^2 - 8u^2) - 3(1 + u^2)^2 \right] \right. \\
& + 3(1 + u^2 - x^2)(1 + 2u^2 + u^4 + 10x^2 - 2u^2x^2 + x^4)L(x, u) \\
& \left. - 24x^2 \left[\arctan(u + x) + \arctan(u - x) \right] \right\}, \quad (20)
\end{aligned}$$

with the auxiliary function $G(x, u)$ defined after eq.(12). The computation of the first two (topologically distinct) diagrams in Fig.8 is done in a similar fashion. In this case one non-elementary integration is left over from the six-dimensional integral over the product of two Fermi spheres of radius k_f . We find the following expression for the isoscalar nuclear spin-orbit strength:

$$\begin{aligned}
U_{ls}^{(3)}(p, k_f) = & \frac{g_A^2 m_\pi^4}{M(4\pi f_\pi)^4 x^3} \int_0^u d\xi \left\{ 4\xi^2 \left[\arctan(u + \xi) + \arctan(u - \xi) \right] \right. \\
& \times \left[(1 + \xi^2 - x^2)L(\xi, x) - x \right] + \frac{ux}{24} \left[9\xi^{-2}(1 + u^2)^2(1 + x^2) - 87\xi^4 \right. \\
& \left. - \xi^2(93 + 146u^2 + 99x^2) - 3(31 + 40u^2 + u^4 + 30x^2 + 38u^2x^2) \right] \\
& + \frac{1}{8}L(\xi, x)L(\xi, u) \left[\xi^6(62x^2 + 57u^2 - 89) - 29\xi^8 + 3\xi^{-2}(1 + u^2)^3(1 + x^2)^2 \right. \\
& + 3\xi^4(12u^2 - 62 - 9u^4 + 8x^2 - 42u^2x^2 - 11x^4) \\
& + \xi^2(69u^2x^4 - 63x^4 + 66u^4x^2 + 294u^2x^2 - 36x^2 - u^6 - 69u^4 - 90u^2 - 154) \\
& \left. - (1 + u^2)(25 + 35u^2 - 2u^4 + 56x^2 + 82u^2x^2 + 2u^4x^2 + 27x^4 + 39u^2x^4) \right] \\
& + \frac{x}{8}L(\xi, u) \left[(1 + u^2)(28 + 41u^2 + u^4 + 27x^2 + 39u^2x^2) - 3\xi^{-2}(1 + u^2)^3(1 + x^2) \right. \\
& + 29\xi^6 + 3\xi^4(20 - 19u^2 + 11x^2) + 3\xi^2(42 + 7u^2 + 9u^4 + 21x^2 - 23u^2x^2) \left. \right] \\
& + \frac{u}{24}L(\xi, x) \left[87\xi^6 + 2\xi^4(90 + 73u^2 - 93x^2) - 9\xi^{-2}(1 + u^2)^2(1 + x^2)^2 \right. \\
& + \xi^2(186 + 266u^2 + 3u^4 + 114x^2 - 260u^2x^2 + 99x^4) \\
& \left. + 6(14 + 17u^2 - u^4 + 31x^2 + 40u^2x^2 + u^4x^2 + 15x^4 + 19u^2x^4) \right] \left. \right\}, \quad (21)
\end{aligned}$$

to which the first and second diagram in Fig.8 have contributed equally. Numerical evaluation of eqs.(20,21) gives at nuclear matter saturation density $k_{f0} = 272.7 \text{ MeV}$ and zero nucleon

²We discard the Hartree-type diagrams resulting from this closing procedure since they have an isospin factor zero in isospin-symmetric nuclear matter.

momentum $U_{ls}^{(3)}(0, k_{f0}) = (-0.20 - 1.10) \text{ MeVfm}^2 = -1.30 \text{ MeVfm}^2$. This is a very small effect compared to iterated 1π -exchange. The momentum dependence of the combined result from eqs.(20,21) for $U_{ls}^{(3)}(p, k_{f0})$ is shown by the dashed line in Fig. 7. One observes a weak increase with momentum from $p = 0$ to $p = k_{f0}$. In the heavy baryon framework the relativistic $1/M$ -corrections calculated here are generated by (nucleon-momentum dependent) vertices from the second order chiral Lagrangian $\mathcal{L}_{\pi N}^{(2)}$ (proportional to $1/M$). The other $\pi\pi NN$ -contact vertices proportional to the low-energy constants $c_{1,2,3,4}$ give rise to spin-orbit terms first one order higher in the small momentum expansion. An order of magnitude estimate of their effect on $U_{ls}(p, k_f)$ can be obtained by inserting the spin-orbit NN-amplitudes $W_{SO}(q)$ and $V_{SO}(q)$ in eqs.(13,15,16) of ref.[13] (which do not include regularization dependent polynomial pieces) into the "master formula" eq.(15).

There are of course many more contributions to the isoscalar nuclear spin-orbit strength at fourth order in small momenta (having the common prefactor m_π^4/M). In order to get an idea about the typical size of other such effects we consider now the first relativistic $1/M$ -corrections to the dominant iterated 1π -exchange Hartree diagrams in Fig.2. In order to obtain conveniently all $1/M$ -corrections from these diagrams one starts with fully relativistic interaction vertices and fully relativistic pion- and nucleon propagators sandwiched between Dirac spinors. Next one performs an expansion in powers of $1/M$ to the appropriate order and solves the remaining (loop)-integrals. In the case of diagram (a) in Fig.2 with one medium insertion one ends up with the following $1/M$ -correction to the isoscalar nuclear spin-orbit strength:

$$\begin{aligned}
U_{ls}^{(a)}(p, k_f)|_{M^{-1}} = & \frac{g_A^4 m_\pi^4}{M(8\pi x)^3 f_\pi^4} \left\{ ux \left(9u^4 + 9x^4 - 6u^2 x^2 + \frac{27 + 43u^2 + 483x^2}{20} \right) \right. \\
& - \frac{2}{5} (28u^5 + 45x^3 + 10u^2 x^3 + 18x^5) \arctan(u+x) \\
& + \frac{2}{5} (28u^5 - 45x^3 - 10u^2 x^3 - 18x^5) \arctan(u-x) \\
& + \left[\frac{7}{2} (3x^2 - u^2) - \frac{27}{20} + \frac{15}{4} (3u^4 + 2u^2 x^2 - 5x^4) \right. \\
& \left. \left. - 9(u^2 - x^2)^2 (u^2 + x^2) \right] xL(x, u) \right\} + \frac{g_A^4 \Lambda k_f^3}{4M(2\pi f_\pi)^4}. \quad (22)
\end{aligned}$$

In this expression we have subtracted the irreducible part $g_A^4 k_f^3 (6\Lambda - 5\pi m_\pi) / (128\pi^4 M f_\pi^4)$ which is already accounted for in eqs.(15,18) by the spin-orbit NN-amplitude $V_{SO}(0)$ derived from the planar 2π -exchange box graph. Inserting the cut-off scale of $\Lambda \simeq 0.65 \text{ GeV}$ one gets $U_{ls}^{(a)}(0, k_{f0})|_{M^{-1}} = (-0.85 + 3.41) \text{ MeVfm}^2 = 2.56 \text{ MeVfm}^2$ which is a small -5% correction to the leading order contribution $U_{ls}^{(a)}(0, k_{f0})|_M = -52.96 \text{ MeVfm}^2$ [7]. The momentum dependence of $U_{ls}^{(a)}(p, k_{f0})|_{M^{-1}}$ is shown by the dashed-dotted line in Fig. 7. One observes a moderate increase with momentum from $p = 0$ to $p = k_{f0}$.

In order to avoid very lengthy analytical expressions, we present here only the first relativistic $1/M$ -corrections to the Hartree diagrams (b) and (c) in Fig. 2 evaluated at zero nucleon momentum ($p = 0$). In the case of diagram (b) one finds:

$$U_{ls}^{(b)}(0, k_f)|_{M^{-1}} = \frac{g_A^4 m_\pi^4 u^2}{M(2\pi f_\pi)^4} \left\{ \left(\frac{15}{8u} - u \right) \arctan u + \frac{4u^6 + 16u^4 - 51u^2 - 45}{24(1+u^2)^2} \right\}. \quad (23)$$

The resulting numerical value $U_{ls}^{(b)}(0, k_{f0})|_{M^{-1}} = -1.06 \text{ MeVfm}^2$ is again a small -3% correction to the leading term $U_{ls}^{(b)}(0, k_{f0})|_M = 37.35 \text{ MeVfm}^2$ [7]. The analogous result for the Hartree

diagram (c) reads:

$$\begin{aligned}
U_{ls}^{(c)}(0, k_f)|_{M^{-1}} = & \frac{g_A^4 m_\pi^4}{M(4\pi f_\pi)^4} \left\{ (6 + 4u^2) \ln(1 + u^2) + 8u(2u^2 - 5) \arctan u \right. \\
& + \frac{u^2(2 - u^2)}{3(1 + u^2)^3} (51 + 133u^2 + 103u^4 + 13u^6) \\
& + \frac{2}{u} \int_0^u d\xi \frac{\xi^4(u - \xi)}{(1 + \xi^2)^4} \ln \frac{u + \xi}{u - \xi} \left[u(2 - u^2)\xi^4 - 5\xi^7 - 20\xi^5 \right. \\
& \left. \left. - 5u^3 + (4u^2 - 27)\xi^3 - 2u(3u^2 + 5)\xi^2 + 4u^2\xi \right] \right\}, \tag{24}
\end{aligned}$$

which leads to an even smaller numerical value of $U_{ls}^{(c)}(0, k_{f0})|_{M^{-1}} = 0.10 \text{ MeVfm}^2$.

In summary, we have calculated here several relativistic $1/M$ -corrections to the isoscalar nuclear spin-orbit strength $U_{ls}(p, k_f)$ generated by chiral 2π -exchange. As expected from chiral power counting these higher order terms are significantly smaller than the unique leading contribution from iterated 1π -exchange [7]. Its role in finite nuclei should be clarified by implementing it into nuclear structure calculations.

References

- [1] O. Haxel, J.H.D. Jensen and H.E. Suess, *Phys. Rev.* **75** (1949) 1766; M. Goeppert-Mayer, *Phys. Rev.* **75** (1949) 1969.
- [2] B.D. Serot and J.D. Walecka, *Adv. Nucl. Phys.* **16** (1986) 1; *Int. J. Mod. Phys.* **E6** (1997) 515; and refs. therein.
- [3] P. Ring, *Prog. Part. Nucl. Phys.* **37** (1996) 193; and refs. therein.
- [4] S. Typel and H.H. Wolter, *Nucl. Phys.* **A656** (1999) 331; and refs. therein.
- [5] F. Hofmann, C.M. Keil and H. Lenske, *Phys. Rev.* **C64** (2001) 034314; and refs. therein.
- [6] N. Kaiser, R. Brockmann and W. Weise, *Nucl. Phys.* **A625** (1997) 758.
- [7] N. Kaiser, *Nucl. Phys.* **A709** (2002) 251.
- [8] N. Kaiser, S. Fritsch and W. Weise, *Nucl. Phys.* **A697** (2002) 255; *Nucl. Phys.* **A700** (2002) 343; and refs. therein.
- [9] A. Bohr and B.R. Mottelson, *Nuclear Structure, Vol.I*, Benjamin, (1969), chapt. 2.4.
- [10] G. Eder, *Kernmaterie*, Spektrum Akademischer Verlag, (1995), chapt. 4.1.
- [11] R.M. Dreizler and E.K.U. Gross, *Density Functional Theory*, Springer Verlag, (1990), chapt. 5.
- [12] J.W. Negele and D. Vautherin, *Phys. Rev.* **C5** (1972) 1472.
- [13] N. Kaiser, *Phys. Rev.* **C64** (2001) 057001.